Journal of Sound and Vibration (1996) **198**(3), 279–298

EXPERIMENTAL STUDY OF A MECHANICAL SYSTEM CONTAINING A LOCAL CONTINUOUS STIFFNESS NON-LINEARITY UNDER PERIODIC EXCITATION AND A STATIC LOAD

T. J. ROYSTON† AND R. SINGH

Acoustics and Dynamics Laboratory, Department of Mechanical Engineering, The Ohio State University, Columbus, OH 43210-1107, *U.S.A.*

(*Received* 17 *January* 1995, *and in final form* 29 *April* 1996)

Local stiffness non-linearities under dynamic (periodic) and static (time-invariant) loads exist in many complex mechanical systems, oftentimes at the junctions of assembled components. Unlike in linear systems, a static load may significantly alter the nature of the non-linearity and dynamic response, in terms of amplitude, frequency content and stability. To examine such phenomena, a controlled laboratory experiment with a local continuous stiffness non-linearity has been designed, fabricated, instrumented and analyzed. It consists of a flexible support structure in the form of a simply supported beam and a rigid body mounted on the support structure by a multi-dimensional non-linear "hardening" spring element. The non-linear elastic element is made of a very thin beam clamped between tapered ends. Multi-harmonic, amplitude-dependent, frequency-sweep-direction-dependent periodic responses to slowly swept harmonic excitation were measured by using order tracking with a dynamic signal analyzer. It was found that the static load induces the "hardening" stiffness element to behave like a "softening" spring under certain conditions. The cause of this is explained via theoretical studies of a simple single-degree-of-freedom non-linear oscillator and a more complex model of the experimental system itself. Experimental and theoretical studies of the multi-degree-of-freedom, multi-dimensional test system also showed that the local non-linearity has a broad spectral and spatial influence on the dynamic behavior of the overall system. For instance, it alters the characteristics of several system resonances and modes.

1. INTRODUCTION

1.1. MOTIVATION

Local stiffness non-linearities exist in many complex mechanical and structural systems, often at the interface or junction of assembled components due to performance requirements, wear or manufacturing tolerances. Non-linear interactions may arise due to finite amplitudes, abrupt changes in material properties or operating conditions, and specific geometrical or kinematic constraints. Examples include bearings [1, 2], sleeve joints [3], slider–crank joints [4], gear mesh interfaces [2, 5, 6], non-linear Hertzian contact regions [7, 8] and vibration mounts [9–13]. Stiffness non-linearities may be the clearance or piecewise linear type (discontinuous) [1, 4–6], continuous [7–13] or may have both discontinuous and continuous regimes [2, 3].

† Present address: Department of Mechanical Engineering, The University of Illinois at Chicago, Chicago, IL 60607-7022, U.S.A.

0022–460X/96/480279 + 20 $25.00/0

Often, the entire physical system, and in particular the non-linear element, may be under the influence of a time-invariant (static) load such as gravity, a preload or mean torque, in addition to dynamic excitation. Such loads may change the static equilibrium of the physical system and the local non-linear element could yield a significantly different elastic force versus displacement relationship. For example, a constraint force–displacement relationship that is symmetric for a zero static load may become significantly asymmetric. This issue will be discussed in this paper, along with the measurement and analysis of periodic vibration in an experimental system that has been carefully designed to exhibit the physical phenomena described above.

1.2. PROBLEM FORMULATION

An assembled system that consists of a rigid body (1) of dimension $N_1(\leqslant 6)$ and a flexible body (2) of dimension N_2 is illustrated conceptually in Figure 1. The flexible body is assumed to be a linear time-invariant dynamic system, and it is connected to the rigid body at a junction (J) via an element containing a local stiffness non-linearity subject to a static load. For the sake of illustration, a simplified physical system is shown in Figure 1(b), where the flexible body (2) is assumed to be a simply supported beam and the rigid body (1) is described by an inertial mass matrix $\mathbf{M}$ with a multi-dimensional displacement vector $\mathbf{x}(t)$. The spring stiffness at (J) is assumed to be a non-linear, continuous function of the relative displacement across the junction. Both static and periodically varying dynamic force excitations, $\mathbf{F}_m$ an $\mathbf{F}_a(t)$, respectively, are present; only the steady state periodic motion is of interest in this paper.

1.3. REVIEW OF THE LITERATURE

Stiffness non-linearities in single-degree-of-freedom systems have been studied in many texts, such as reference [14]. For the case of the continuous symmetric stiffness non-linearity of the polynomial type, a static load may effectively make the stiffness asymmetric, hardening in one direction and softening in the other, due to the shift in the equilibrium point. This issue has been indirectly treated by considering quadratic and quadratic-plus-cubic-stiffness non-linearities in systems with zero static loads. For example, it has been found that a quadratic non-linearity may have a "softening" effect on the system response, regardless of its sign, since it shifts the dynamic operating point

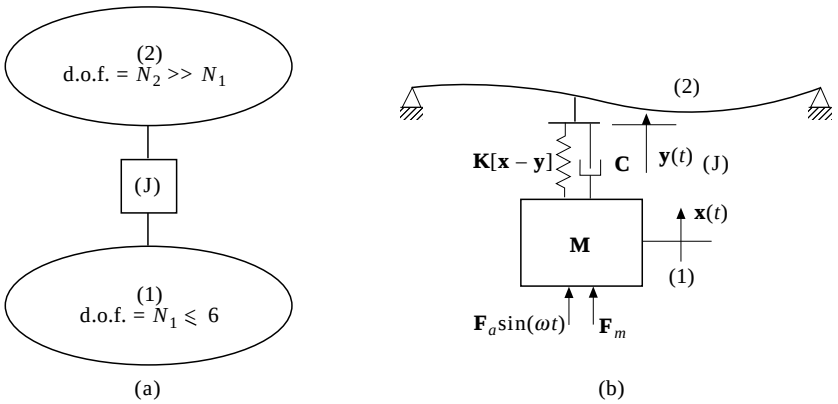

Figure 1. A built-up structure consisting of rigid (1) and flexible (2) bodies connected through a local non-linearity (J). Here, N_1 and N_2 refer to the number of degrees of freedom in components (1) and (2). (a) Conceptual model; (b) example case: rigid body connected to a simply supported beam through a non-linear stiffness element.

in the softening direction along the force versus displacement curve [14]. For the case of a discontinuous stiffness non-linearity, investigators have shown theoretically that the influence of a static load on the system response can be quite different. In fact, even when the stiffness characteristics are very similar to a continuous one, e.g., piecewise linear approximations to polynomial curves, the resulting dynamic response will include very different frequency response curves and jump phenomena [15]. Experimental investigations of single-degree-of-freedom systems with discontinuous stiffness non-linearities, such as a recent study of a torsional gear pair by Blankenship and Kahraman [16], have supported these findings.

Of course, standard experimental techniques based on the transfer function and modal analysis concepts are not applicable to non-linear systems. In addition to the study cited above, which dealt specifically with the issue of a statically loaded stiffness non-linearity, several recent experimental studies of non-linear systems are reviewed as a part of this paper, in order to introduce the techniques that have been successful and the dynamic behavior that must be considered [16–20]. Zaretzky and Crespo de Silva [17] measured non-linear coupling in orthogonal modes of vibration (whirling), and multiple stable solutions for a given excitation frequency and amplitude (hysteresis), in a base-excited, vertical cantilever beam. They noted the need to use sinusoidal excitation, as opposed to random excitation, as some non-linear responses take time to reach steady state. In a similar study by Zavodney and Nayfeh [18], where the beam carried a lumped mass, it was noted that certain non-trivial solutions had small domains of attraction. Specifically, the steady state response of large amplitude for a stiffness-hardening resonance could only be excited by starting at a lower excitation frequency and then slowly increasing the frequency. Hanson *et al*. [19] observed modal coupling and multiple stable solutions for a wide range of excitation levels in a vibrating wire under electromagnetic transverse excitation. The need to study more carefully higher harmonics in the system response was mentioned. Valkering [20] has considered the transverse vibration of an end-forced string with an impact non-linearity, in the form of a stop located at the string's mid-point. Multiple stable solutions, bifurcations and transitions from periodic to chaotic motion were observed. This study shows that a localized non-linearity can significantly affect a spatially extended system. In a recent study of a single-degree-of-freedom geared system, Blankenship and Kahraman [16] used the "orders domain" with a dynamic signal analyzer to obtain response information as a function of shaft angular rotation.

1.4. OBJECTIVES

On the basis of the literature review, a clear need exists for an experimental study of a complex mechanical system with a local stiffness non-linearity under both periodic (dynamic) and time-invariant (static) excitations. The effect of the non-linearity and the variation of this effect due to the static load on phenomena peculiar to multi-degree-of-freedom systems, including multiple resonant frequencies and mode shapes, needs to be experimentally assessed and disseminated to the theoretical investigators. A logical approach to the experimental analysis of the steady state periodic response of non-linear mechanical systems appears to be the use of harmonic excitation with slowly varying frequency, both increasing and decreasing, and measurement of the multi-harmonic response of numerous response variables throughout the system.

Specific objectives of this study are: (1) to examine theoretically issues with respect to a static load and the resulting asymmetry in stiffness by way of a single-degree-of-freedom simplification of the system of Figure 1; (2) to design an experiment with a local non-linearity under a static load that incorporates physical phenomena described above

and by Figure 1 and extends the aforementioned theoretical study to the case of a multi-degree-of-freedom, multi-dimensional system; (3) to fabricate and instrument the experiment to capably capture the non-linear periodic system response; and (4) to validate and interpret the measured data by using simplified non-linear models of the experiment. The scope of this paper is limited to a continuous hardening-type spring in the presence of a static load (gravity), and only the steady state periodic vibration response is considered.

2. THEORETICAL EXAMINATION OF AN ASYMMETRIC STIFFNESS NON-LINEARITY

The effect of a static load on a continuous stiffness non-linearity is first examined by considering a single-degree-of-freedom system under harmonic and static excitations. Assume that the beam of Figure 1(b) is very stiff and acts like a rigid based ($N_2 = 0$). With vertical motion only ($N_1 = 1$), the resulting system is described by

$$M\ddot{x}(t) + C\dot{x}(t) + F_k[x(t)] = F_m + F_a \sin(\omega t), \qquad F_k[x] \equiv K[x]x, \tag{1}$$

where M is the mass, C is the viscous damping coefficient, F_k is the non-linear elastic force, F_m is the static load and F_a is the amplitude of the dynamic excitation at frequency ω. Several cases of equation (1) will be discussed next.

2.1. ASYMMETRIC SPRING

Assume that F_k is described by the following in the absence of a static load ($F_m = 0$):

$$F_k \equiv k[1 + \beta|x|x]x. \tag{2}$$

The stiffness is essentially hardening in one direction and softening in the other direction about the origin $x = 0$. This direction depends on the sign of β, as illustrated in Figure 2b. How the system will dynamically respond to harmonic excitation, hardening or softening (or neither), may not be intuitively obvious.

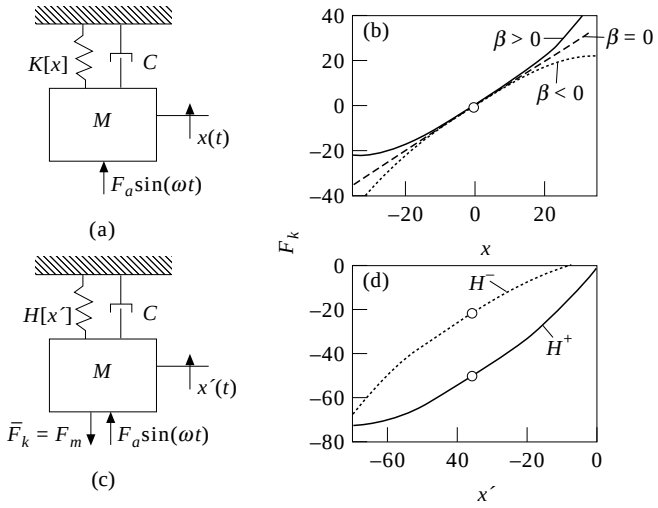

Figure 2. The effect of a static load on a single-degree-of-freedom non-linear system. (a) Asymmetric stiffness and zero static load; (b) equivalent hardening and softening stiffness characteristics; (c) the system in the presence of a static load ($F_m = -\bar{F}_k$); (d) force–deflection relationship corresponding to (c). ○, static operating point.

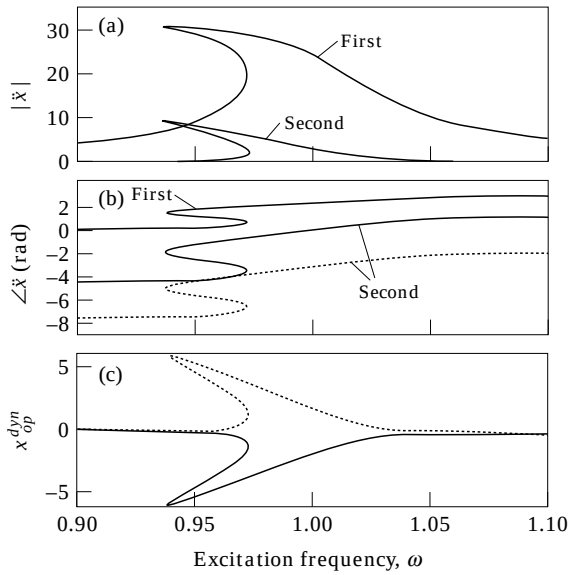

Figure 3. The frequency response of single-degree-of-freedom non-linear system described by equation (1). ——, $\beta > 0$; . . ., $\beta < 0$. (a) Magnitude (identical for all harmonics); (b) phase (identical for odd harmonics, π radians out of phase for even harmonics); (c) the dynamic variation of the operating point x_{op}^{dyn} (zeroth harmonic).

The frequency response for a specific configuration was solved for using the Galerkin method (multi-term harmonic balance) [21] with arbitrary values of $M = k = F_a = 1$, $C = 0{\cdot}03$ and $\beta = +0{\cdot}0003$. Integer order harmonics are found in the response and sample solution curves are shown in Figures 3 and 4. As may have been intuitively expected, there is no difference in the magnitude of the response using either the positive or negative value of β. However, there is a difference in the phase of the response for the even harmonics which is clearly evident in the time domain. Perhaps, it is less obvious that the response should be dynamically softening. However, the variation of the dynamic operating point x_{op}^{dyn} (the static component in the multi-term harmonic balance) shown in Figure 3(c)

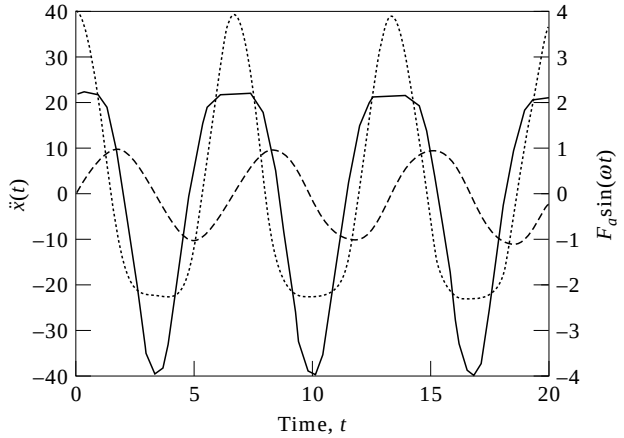

Figure 4. The time domain response of the single-degree-of-freedom non-linear system described by equation (2) at excitation frequency $\omega = 0{\cdot}94$ (large amplitude solution). ——, $\ddot{x}(t)$ given $\beta > 0$; · · ·, $\ddot{x}(t)$ given $\beta < 0$; - - -, $F_a \sin(\omega t)$.

indicates that the system "favors" operation in the softening regime near the system resonance. Such a bias is also evident in the time response shown in Figure 4. This tendency seems logical since there is less resistance to motion in the "softening" direction and the dynamic operating point shifts in this direction with amplitude, resulting in a backbone curve bent towards lower frequencies.

2.2. CHANGE IN STATIC EQUILIBRIUM GIVEN $F_m \neq 0$

The static equilibrium point ($\bar{x}$) will be affected when a static load F_m is introduced. Redefine the dynamic variable as x', where $x' = x - \bar{x}$, as shown in Figure 2(b). Corresponding to x', one defines F'_k, where $F'_k = F_k - \bar{F}_k$ and $\bar{F}_k = k(1 + \beta|\bar{x}|\bar{x})\bar{x}$. Substituting x' for x in equation (2) and subtracting $\bar{F}_k$, one obtains

$$F'_k = kx' + \begin{cases} -k\beta[(x' + \bar{x})^3 + |\bar{x}|\bar{x}^2], & x' \leqslant -\bar{x}, \\ k\beta[(x' + \bar{x})^3 - |\bar{x}|\bar{x}^2], & x' \geqslant -\bar{x}. \end{cases} \tag{3}$$

Thus, as a function G of x' one has

$$F'_k = G[x'] = \begin{cases} G_1[x'^0, x', x'^2, x'^3], & x' \leqslant -\bar{x}, \\ G_2[x'^0, x', x'^2, x'^3], & x' \geqslant -\bar{x}. \end{cases} \tag{4}$$

Next, equation (1) is rewritten in terms of x' as follows:

$$M\ddot{x}'(t) + C\dot{x}'(t) + G[x'(t)] = F_a \sin(\omega t) - \bar{F}_k. \tag{5}$$

Thus, with respect x', one effectively has a static load of the form $F_m = -\bar{F}_k$. An equivalent system to that of Figures 2(a) and (b) is shown in Figures 2(c) and (d). Due to the equivalency of the systems, one can directly reason that, as before, the sign of β has no impact on the amplitude of response, but just on its phase. Thus, all four systems, whether using either positive or negative β and x or x' yield exactly the same dynamic response in magnitude.

2.3. "SOFTENING" VERSUS "HARDENING" EFFECTS

The multi-functional expression for $G[x']$ in equation (4) can be approximated by a unifunctional expression $H[x']$. The approximation needs to be accurate only over the range of values x' that are reached for a particular excitation F'_k. Now consider the case in which $|x'(t)| < |\bar{x}|$ for any t. By examining the nature of $H[x']$ for both positive and negative β; a least squares fit with a third order polynomial yields the following expression for the example case with $\bar{x} = 36$:

$$H^+[x'] = \sum_{i=0}^{3} a_i^+ x^i \qquad \text{for } \beta = +0{\cdot}0003 \text{ and } \bar{F}_k = 50{\cdot}0, \tag{6a}$$

where $a_0^+ = 2{\cdot}19$, $a_1^+ = 3{\cdot}74 \times 10^{-2}$, $a_2^+ = 5{\cdot}71 \times 10^{-4}$ and $a_3^+ = 3{\cdot}87 \times 10^{-6}$;

$$H^-[x'] = \sum_{i=0}^{3} a_i^- x^i \qquad \text{for } \beta = -0{\cdot}0003 \text{ and } \bar{F}_k = 22{\cdot}0, \tag{6b}$$

where $a_0^- = -0{\cdot}186$, $a_1^- = -3{\cdot}74 \times 10^{-2}$, $a_2^- = -5{\cdot}71 \times 10^{-4}$ and $a_3^- = -3{\cdot}87 \times 10^{-6}$.

The two expressions are shown in Figure 2(d). Note that the first is essentially a softening stiffness model and the second is a hardening stiffness model with respect to the operating

point at $x' = 0$. Recall, though, that both yield an identical magnitude of response and both produce a dynamically softening response. Hence, based on this simple study, it is observed that a static load in combination with a continuous symmetric stiffness non-linearity may yield a softening dynamic response, regardless of whether the stiffness is hardening or softening. This occurs because the static load induces an asymmetry in force–displacement characteristics with a change in the operating point. This interesting observation is utilized in the next section in, which an experimental system is considered.

3. EXPERIMENTAL STUDY

A multi-degree-of-freedom, multi-dimensional experimental system was designed and constructed. The system consists of a statically loaded continuous stiffness non-linearity connecting flexible and rigid bodies, in accordance with the discussion of the previous sections.

3.1. DESCRIPTION OF THE SYSTEM

A diagram of the experimental set-up is shown in Figure 5. In order to approximate a simply supported beam, two cast iron mounting structures (d) with masses of about 150 kg each were chosen as a fixed reference frame. These were isolated from the floor using 100 mm thick Neoprene rubber (f). Simply supported end conditions (a) for the rectangular beam were simulated by using thin brass shims which connect the beam to the fixed reference frame. The shims restrict translational motion at the beam ends but provide

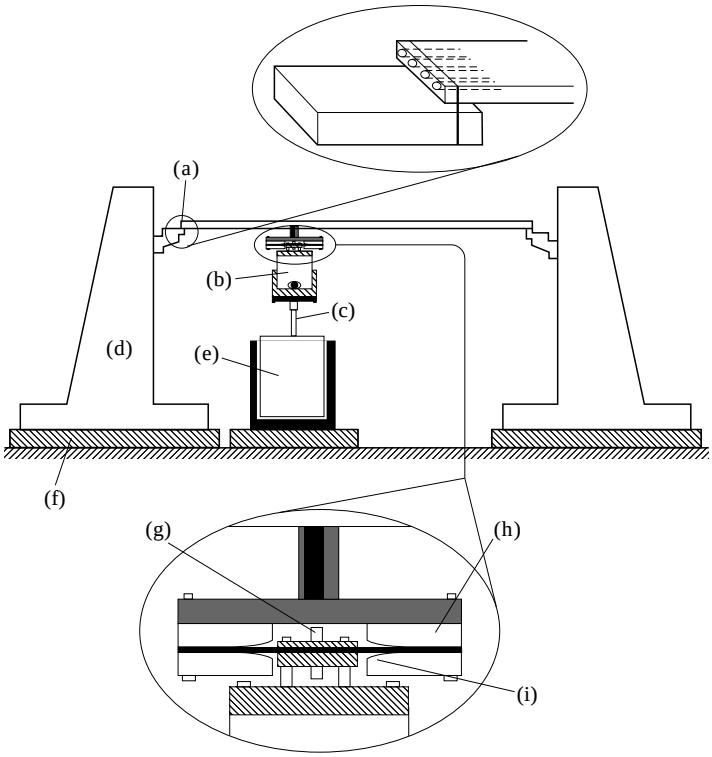

Figure 5. A schematic of the experimental set-up. (a) Simply supported beam; (b) rigid body; (c) external force input; (d) fixed base; (e) excitation (electrodynamic shaker); (f) Neoprene rubber; (g) proximity probe; (h) non-linear stiffness hardening element; (i) curvature exaggerated.

TABLE 1

List of instrumentation

Item	Manufacturer and model number
Impedance heads	PCB Piezotronics, Inc. number 288M17
Electrodynamic shaker	VTS, Inc., number VG 100/6
Accelerometers	PCB Piezotronics, Inc., number A353B17
Signal conditioners	PCB Piezotronics, Inc., number 480E09
Dynamic signal analyzer	Hewlett-Packard, number 3566a w/Opt. 35636a
Inductive proximity probe	Electro-Mike 3/16 inch
Swept or fixed sinusoidal excitation source	Hewlett-Packard, number 35665a w/Opt. 1D2
Power amplifier for shaker	Electro Voice, number 7300A

minimal resistance to rotational motion. The non-linear stiffness element was bolted to and hung from the simply supported beam through an impedance head which provided measurement of the vertical acceleration and force (refer to Table 1 for a list of equipment and instrumentation). The non-linear element (h) consisted of a small thin aluminum beam spring sandwiched between thicker (rigid) aluminum blocks. The rigid ends have slight tapers in their surface profile (i) produced by sanding, which effectively varies the length of the aluminum beam spring as it deflects. It was patterned after Den Hartog's description of a cantilever beam spring that becomes stiffer for larger deflections [22]. The rigid body (b) was excited by the electrodynamic shaker (e) through another impedance head. Additional accelerometers and an inductive proximity probe (g) were used to obtain measurements of other system variables. Up to eight measurements were taken simultaneously with a dynamic signal analyzer. Physical parameter values for the experiment, measured or estimated, are provided in Table 2.

3.3. THEORETICAL MODEL

For the simply supported beam, the dynamics can be described by Euler's beam equation [23]:

$$\rho A\ddot{u}(s, t) + EI\frac{\partial^4 u}{\partial s^4}(s, t) = F_y(t)\delta(s - s_b) - m_y\ddot{u}(s, t)\delta(s - s_b). \tag{7}$$

Here, ρ, A, E, I, δ, s_b, m_y and F_y refer to the material density, the cross-sectional area, Young's modulus, the moment of inertia, the Dirac delta function, the axial position of the non-linear element connection to the beam, the mass of the rigid components connecting the non-linear stiffness element to the beam and the vertical constraint force across the non-linear element, respectively. Modal decomposition is performed to obtain N_w coupled, ordinary differential equations. Given a force excitation $F_y(t) = \tilde{F}_y\, e^{i\omega' t}$ at an

TABLE 2

Measured or estimated physical parameters of the experiment

$A = 6.45 \times 10^{-4}\ m^2$	$l_s = 0{\cdot}508$ m	$s_b = 3l_s/8$
$E = 7.1 \times 10^{-10}\ N/m^2$	$M = 3{\cdot}307$ kg	$\xi = 0{\cdot}01$†
$g = 9{\cdot}8\ m/s^2$	$m_y = 0{\cdot}2356$ kg	$\rho = 2714{\cdot}3\ kg/cm^3$
$h = 6{\cdot}35$ mm	$N_w = 6$	
$\zeta_{i=1,\ldots,6} = 0{\cdot}02, 0{\cdot}004, 0{\cdot}004, 0{\cdot}004, 0{\cdot}008, 0{\cdot}01$‡		

† With respect to the linear stiffness coefficient in equation (13).

‡ Based on experimental modal analysis.

arbitrary frequency ω', the response expressions are as follows, where l_s refers to the length of the beam and ζ_j is the proportional modal damping ratio:

$$u(s, t) = \sum_{j=1}^{N_w} \tilde{u}_j \sin\left(\frac{j\pi s}{l_s}\right) e^{i\omega' t}, \tag{8}$$

which yields

$$m_b \tilde{\mathbf{\Psi}}(\omega') \begin{bmatrix} \tilde{u}_1 \\ \vdots \\ \tilde{u}_{N_w} \end{bmatrix} = \mathbf{H}^T \tilde{F}_y, \qquad \text{where } \tilde{\mathbf{\Psi}} \equiv \begin{bmatrix} \tilde{\Psi}_1 + \Theta_{1,1} & \cdots & \Theta_{1,N_w} \\ \vdots & \ddots & \vdots \\ \Theta_{N_w,1} & \cdots & \tilde{\Psi}_{N_w} + \Theta_{N_w,N_w} \end{bmatrix},$$

$$\Psi_j(\omega') \equiv \omega_j^2 - \omega'^2 + i2\zeta_j \omega' \omega_j, \qquad \Theta_{j,k}(\omega') \equiv -\mu_y \omega'^2 \sin(j\pi s_b/l_s) \sin(k\pi s_b/l_s),$$
$$\mathbf{H} \equiv [\sin(\pi s_b/l_s) \cdots \sin(N_w \pi s_b/l_s)], \qquad \omega_j \equiv \sqrt{EI/\rho A}\,(j\pi/l_s)^2,$$
$$m_b \equiv \rho A l_s/2, \quad \mu_y \equiv m_y/m_b, \qquad j, k = 1, \ldots, N_w. \tag{9}$$

From equations (8) and (9), it follows that

$$\tilde{y} = \mathbf{H}[\tilde{u}_1 \cdots \tilde{u}_{N_b}]^T, \qquad \tilde{T}_y(\omega') \equiv \frac{\tilde{y}}{\tilde{F}_y}(\omega') = \frac{1}{m_b} \mathbf{H} \tilde{\mathbf{\Psi}}^{-1}(\omega') \mathbf{H}^T, \tag{10a, b}$$

For the non-linear stiffness element and rigid mass, one has the following expressions:

$$a^U \sin(\omega t) - Mg - F_y(t) - M\ddot{x}(t) = 0, \tag{11a}$$

$$F_y(t) = K[x - y](x(t) - y(t)) + 2\xi\sqrt{MK}(\dot{x}(t) - \dot{y}(t)). \tag{11b}$$

The constraint force across the non-linear element $F_y(t)$ includes elastic and dissipative terms. The damping is assumed to be linear viscous with a damping ratio ξ that is estimated based on a comparison to experiment under the dynamic excitation conditions discussed in section 4. A rough estimate of the non-linear stiffness expression can be made on the basis of the system geometry. Referring to Figure 6(a), the element is approximated as a simply supported beam with length l_b which is dependent on relative displacement $(x - y)$ through the expressions

$$l_b = l_c - l_p - 2l_d, \qquad l_d = l_d[d], \qquad d \approx \frac{2l_d}{l_c - l_p}(x - y), \tag{12a–c}$$

where d and l_d are related by the taper profile shown in Figure 6(b). This profile was measured using a computer-aided 3-D co-ordinate measurement machine. For the calculations, an average of the two lower block profiles was used, since the upper blocks (which had similar profiles) did not come into play during the dynamic excitation studies discussed in Section 4. Given a value of l_d, d is found based on the profile and a corresponding values of l_b and $x - y$ are calculated. The stiffness $K[x - y]$ of the non-linear element is estimated based on reference [22] as $K = 48EI/l_b^3$ for the range of relative displacement values $x - y$ reached during dynamic excitation studies. This relationship is then approximated using a sixth order polynomial expression based on a least squares fit. The sandwiched plate mounted at the center of the beam is sufficiently thick to be considered as a rigid concentrated mass. The first natural frequency for the simply supported beam with its length l_b at a maximum value of $l_c - l_p$ is estimated to be 1080 Hz. Hence the approximation of the non-linear element simply with its static stiffness value was judged to be sufficient for the frequency range considered.

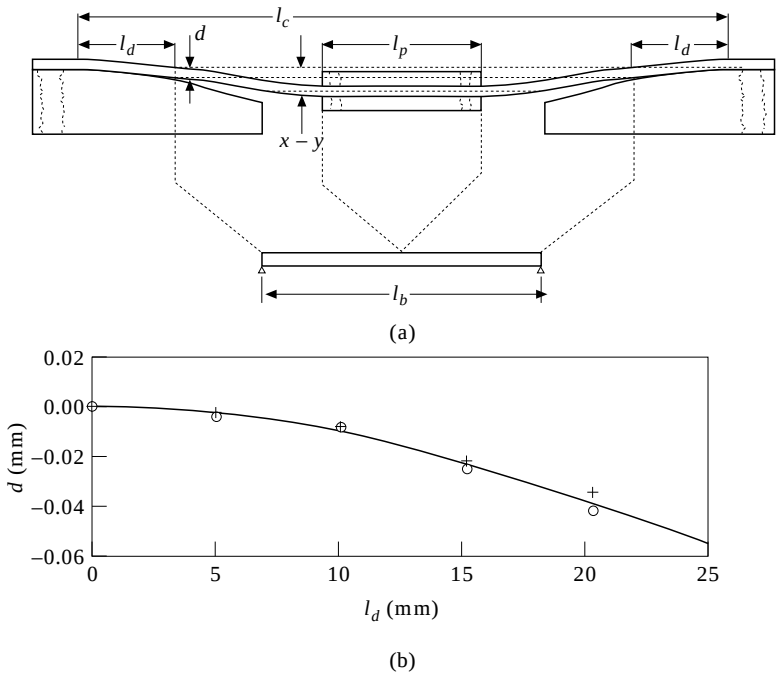

Figure 6. A profile of the non-linear stiffness element. (a) Schematic diagram; (b) measured taper profile: ○, Left lower block; +, right lower block; ——, polynomial curve fit to average.

The resulting force versus deflection relationship of Figure 7 indicates a symmetric hardening stiffness about the origin. However, as shown in Section 2, this becomes an asymmetric stiffness, hardening in one direction and softening in the other, due to the static gravitational force $(-Mg)$ which changes the system operating point as shown in the figure.

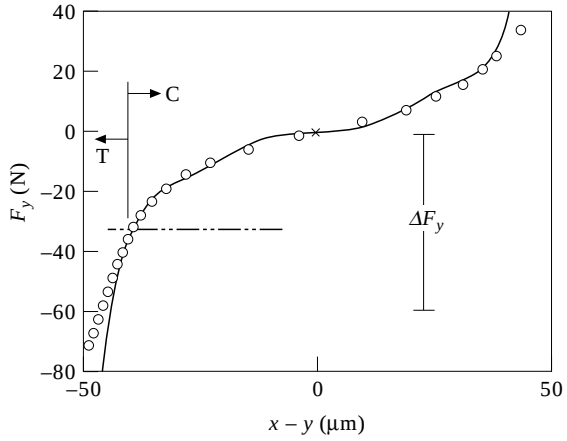

Figure 7. The static force versus deflection for vertical displacement across the non-linear stiffness element. Here, regime T denotes the tension test range, regime C denotes the compression test range, x is the static operating point without gravity load, line —· ·— is the static operating point with gravity load, and ΔF_y is the operating range of the dynamic studies discussed in section 4. ○, Static experimental measurements; ——, theoretically predicted.

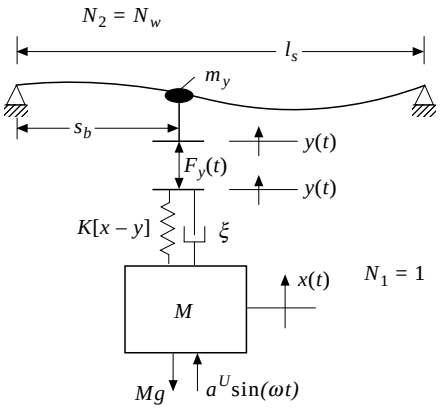

Figure 8. A simplified model of the experimental system of Figure 5.

The overall theoretical system model is shown in schematic form in Figure 8. Note that in the experiment, the stiffness element was intentionally *not* placed at the mid-point of the beam ($s_b/l_s \neq 1/2$). While this theoretical model and an even more complex model that considers multi-dimensional motion suggest that such a placement would result in excitation of odd beam modes only and vertical system motion only, in practice this is not the case. Any misalignment in the system, which was unavoidable, results in a non-vertical excitation component and non-vertical motion of the rigid mass which, in turn, excites the even order modes of the simply supported beam through moment coupling. Hence, better agreement in response between theory and experiment was obtainable only when the mount footing was *not* located at an antinode of a simply supported beam mode that resonated in the frequency range of interest.

In a companion paper [24], the authors have presented an efficient analytical and computational framework for the solution of the resulting non-linear equations. Development of the framework, based on the Computational Galerkin method, is not repeated here; only the specific results when applied to the experiment are presented.

3.4. MEASUREMENT OF SYSTEM PARAMETERS AND VERIFICATION OF THEORY

An experimental modal analysis of the simply supported beam was conducted. The experimental method for approximating the simply supported boundary conditions has worked excellently for the first several modes based on comparisons of natural frequencies and mode shapes to theoretical values obtained via Euler's beam theory, as given in Table 3. Modal analysis of the beam with the rigid component that connects the non-linear

TABLE 3

Natural frequencies of the simply supported beam

Experiment, $\omega/2\pi$ (Hz)	Euler's beam theory, $\omega/2\pi$ (Hz)
57	57
228	228
512	514
912	913
1470	1427
2100	2050

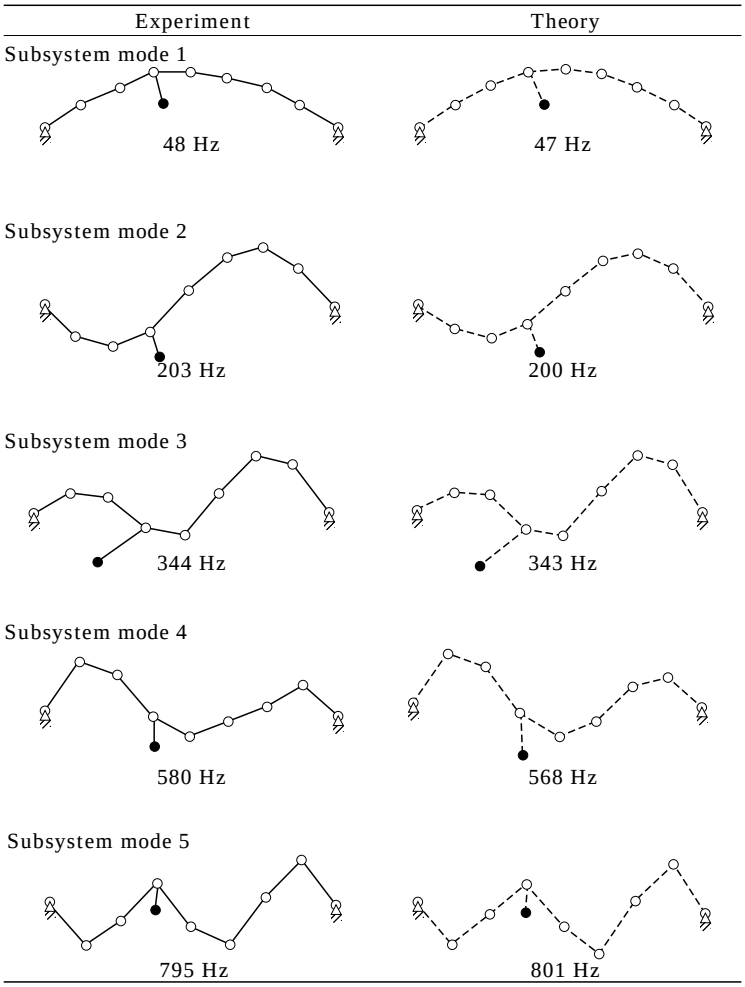

Figure 9. Experimental and theoretical mode shapes and natural frequencies of the simply supported beam subsystem.

stiffness element to the beam was also undertaken. Indeed, approximating this component as a lumped mass on the beam is a simplification. A more accurate model that accounts for pivoting motion of the rigid component about its connection point to the beam is easily formulated. It compares well with experiment, as seen in Figure 9. However, this multi-dimensional model could not be used for studies of the entire non-linear system, because a corresponding model for the rotational stiffness across the non-linear element cannot be easily solved theoretically or estimated experimentally. The repercussions of this simplification in the theoretical model are discussed in Section 4.2.

The non-linear element and rigid body are considered together for a static measurement of the non-linear vertical stiffness term $K[x - y]$. Static force versus deflection relationships were experimentally obtained by placing the system under tension and compression, as shown in Figure 10. The measured relationship, shown in Figure 7, compares well with predictions, supporting the validity of the theoretical approach undertaken.

Shown in Figure 11 are force versus deflection characteristics for two different polynomial stiffness models, one with a softening non-linearity and one with a hardening

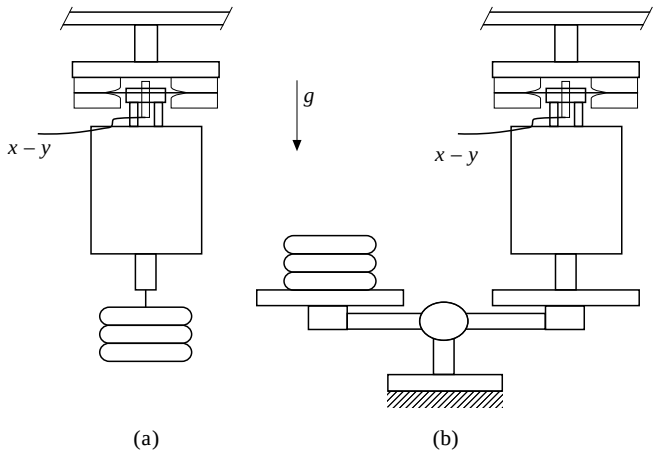

Figure 10. Measurement of the vertical force versus deflection $x - y$ across the non-linear stiffness element. (a) Tension (T) test; (b) compression (C) test.

non-linearity. The softening model was estimated based on the dynamic studies discussed in Section 4. The linearized stiffness was determined by matching theory to experiment for very low excitation levels. Then, based on studies at higher excitation levels, a non-linear term was added. The softening relationship shown in Figure 11 is given by the expression

$$F_y = a[1 - b|x - y|^{2\cdot5} \text{ sign } (x - y)](x - y), \tag{13}$$

where $a = 2{\cdot}22 \times 10^6$ and $b = 1{\cdot}23 \times 10^6$, for $x - y$ in meters and force in Newtons. Next, using an approach similar to the one used in Section 2, a dynamically equivalent hardening stiffness model was obtained, this time for the same static load condition ($-Mg$). It is given by the polynomial expression

$$F_y = \sum_{i=1}^{5} Ka_i(x - y)^i, \tag{14}$$

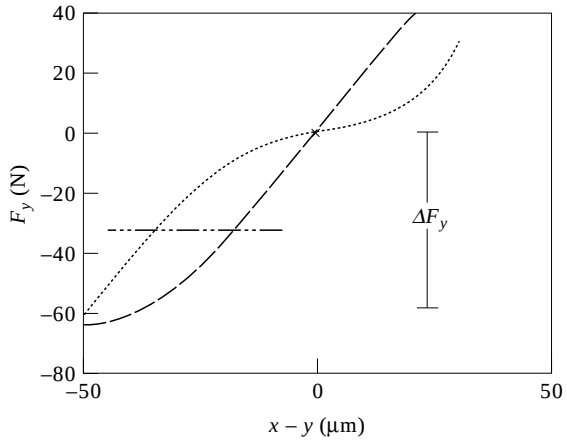

Figure 11. Force versus deflection models for vertical displacement across the non-linear stiffness element based on dynamic studies over the operating range ΔF_y. Here, x denotes the static operating point without gravity load, and line —· ·— is the static operating point with gravity load. — —, Polynomial softening stiffness model; . . ., equivalent polynomial hardening stiffness model.

where $K = 2{\cdot}74 \times 10^5$, $a_1 = 1$, $a_2 = 3{\cdot}62 \times 10^4$, $a_3 = 4{\cdot}48 \times 10^9$, $a_4 = 6{\cdot}04 \times 10^{13}$ and $a_5 = 2{\cdot}29 \times 10^{17}$. This curve qualitatively agrees well with the theoretical and statically measured force versus deflection relationships shown in Figure 7. It should be pointed out here that, as indicated in Figure 11, the dynamic equivalence of the hardening and softening stiffness models is only valid over the operating range ΔF_y, which does not extend beyond $|x - y| = 0$.

4. DYNAMIC MEASUREMENTS

4.1. METHODOLOGY

Based on the review of the literature, the following test methodology was adopted for dynamic studies. The experimental system was driven by harmonic excitation, swept up and down in frequency at a rate of 0·5 Hz/s. Decreasing the sweep rate any further did not alter the response; i.e. steady state was still achieved. An eight channel dynamic signal analyzer and an array of force transducers and accelerometers were used to record the system response. Impedance heads provided direct measurement of the vertical dynamic excitation force $U(t)$ and response acceleration $\ddot{x}(t)$ at the excitation location and the vertical response force $F_y(t)$ and acceleration $\ddot{y}(t)$ at the interface between the non-linear element and the simply supported beam. Additional transducers provided measurement of the horizontal motion of the system and the beam response.

Measurement of periodic response to sinusoidal excitation, including sub- and super-harmonic components, was made possible via the order tracking capability of the dynamic signal analyzer, which is commonly used for the analysis of rotating machines. The principle is as follows [25]. A tachometer signal enables the spectrum analyzer to sample data using increments of rotation in place of fixed time increments. The order number refers to the harmonic number normalized to one revolution of the system. Thus, if the system rotational speed drifts within a single rotation or from rotation to rotation, the sampled time points will still correspond to equally spaced rotational angles of the system. If insufficient tachometer pulses occur per revolution to satisfy the Nyquist criteria for measurement up to a desired order, additional sampling points between pulses are added via interpolation. For this experiment, the entire process is simulated by using the swept sine excitation signal in place of the tachometer to establish the order domain. Measurement system parameters are set so that one (tachometer) pulse is recorded per period (revolution) of the excitation. Additional sampling points per period are interpolated as needed. Since the excitation frequency ω is varied slowly, the analyzer is able to perform a very accurate spectral analysis of the system, providing measurement of up to five sub- or superharmonics at a time as a function of the swept frequency. The excitation force input is taken as the phase reference and cross- and auto-spectrum values of the measured system signals at each selected $j\omega/k$ (where j and k are integers) are calculated by the analyzer.

Here, one denotes the auto- and cross-spectra of a signal q for the jth order harmonic of the kth order subharmonic as $Au[\tilde{q}(j\omega/k)] \equiv \tilde{q}(j\omega/k)^*\tilde{q}(j\omega/k)$ and $Cr[\tilde{q}(j\omega/k)] \equiv \tilde{q}(j\omega/k)^*\tilde{U}(j\omega/k)$, where the superscript tilde and asterisk denote a complex value and a complex conjugate, respectively. From these values, the amplitude of the response of q can be estimated as a function of ω at any sub- or superharmonic, i.e., $j\omega/k$. Phase information for q at a particular harmonic relative to the phase of the excitation force at that particular harmonic is also available. For Figures 12, 14 and 15 below, the amplitude of the frequency

response of $\ddot{y}$ at the jth harmonic with respect to the dynamic excitation F_a at the primary harmonic ($j = 1$) is calculated from experimental data using the expression

$$|\ddot{y}/U| = \sqrt{Au[\ddot{\tilde{y}}(j\omega)]/Au[\tilde{U}(\omega)]}. \tag{15}$$

4.2. RESULTS AND DISCUSSION

In this paper, the range of excitation frequencies is restricted to between 150 and 350 Hz. Measurement of the dynamic input force signal $U(t)$ indicated that the excitation was nearly harmonic with minimal distortion or higher harmonic content; however, it was not constant in amplitude as a function of frequency. Constant excitation voltage amplitude to the electrodynamic shaker did not equate to constant excitation force amplitude to the test system. This was taken into account in computer simulation studies which used the experimentally measured excitation amplitude–frequency relationship as an input. (A signal feedback feature of the source signal generator for obtaining a constant excitation force level was not used, since it exhibited instability due to jumps in the response).

In Figures 12–15, the measured system response from $\omega/2\pi \approx 150$ Hz to 350 Hz is shown. Non-linear phenomena including amplitude-dependence, frequency-sweep-direction-dependence and strong superharmonic content, are evident. The (subharmonic response in both the experimental measurements and theoretical simulations was found to be negligible). The strong resonance at $\omega/2\pi \approx 165$–170 Hz that is highlighted in Figure 12 is due primarily to excitation of the second beam mode coupled with vertical translational and minor rotational motion across the mount. Theoretical predictions using the dynamically identical softening and hardening stiffness model of equations (13) and (14) qualitatively agree with the experimental measurement showing a strongly non-linear softening resonance. In the physical system, the static gravitational load has rendered the

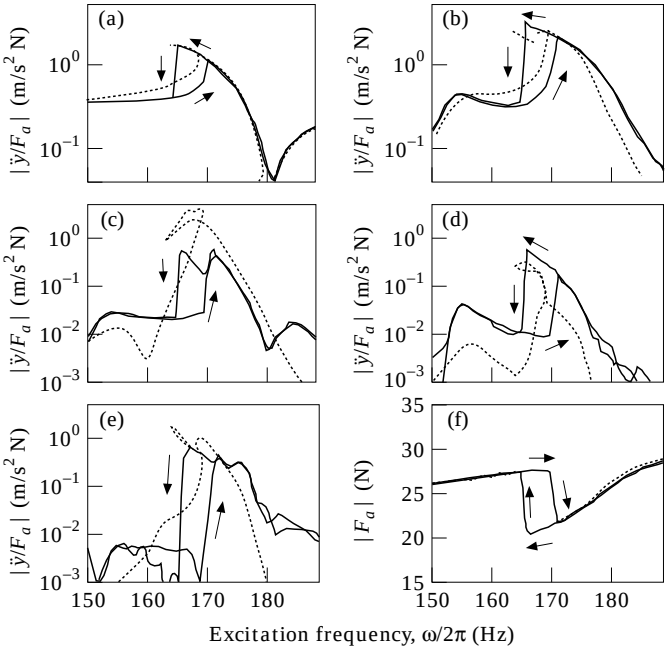

Figure 12. Order tracking measurements of $\ddot{y}(\omega)$ compared to theory for swept harmonic excitation. (a) First harmonic; (b) second; (c) third; (d) fourth; (e) fifth; (f) excitation (harmonic). ——, Experiment; · · ·, theoretical model.

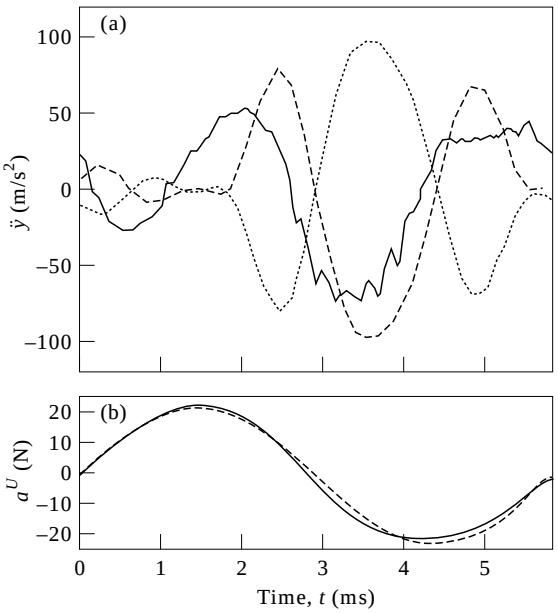

Figure 13. A time domain response comparison of the large amplitude solution to the excitation force $U(t)$ at $\omega/2\pi = 171$ Hz. (a) ——, Experimental value of $\ddot{y}(t)$; · · ·, theoretical value of $\ddot{y}(t)$ using the softening stiffness model; - - -, theoretical value of $\ddot{y}(t)$ using the equivalent hardening stiffness model. (b) Excitation force: ——, experiment; - - -, theory (both stiffness models).

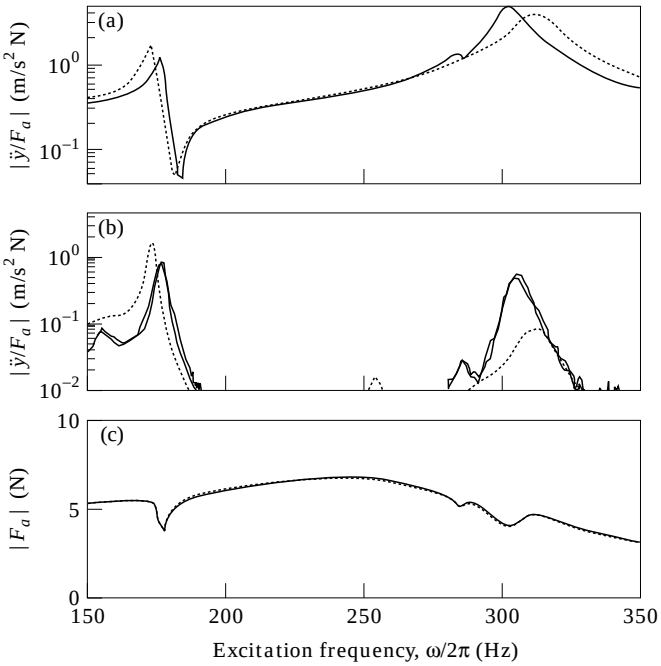

Figure 14. Order tracking measurements of $\ddot{y}(\omega)$ compared to theory for swept harmonic excitation of a lower amplitude. (a) First and (b) second harmonics; (c) excitation (harmonic): ——, experiment; . . ., theoretical model.

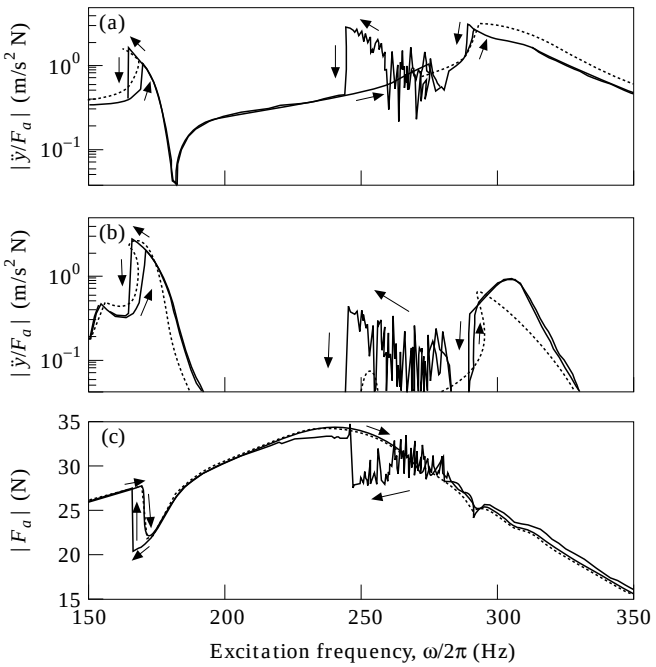

Figure 15. Order tracking measurements of $\ddot{y}(t)$ compared to theory for swept harmonic excitation of higher amplitude. (a) First and (b) second harmonics. (c) Excitation (harmonic). ——, Experiment; · · ·, theoretical model.

hardening stiffness asymmetric. As in the theoretical study, this asymmetry results in a dynamically softening response. Either the softening or hardening stiffness models in combination with a static load can be used to simulate this response.

Unlike in the theoretical study of Section 2, the experiment is a multi-degree-of-freedom system. Some issues with respect to this phenomenon are considered. Note that the response at the second harmonic is comparable in magnitude to the fundamental harmonic. This is clearly shown in the time domain plot of Figure 13. A system resonance at 310 Hz associated with out-of-phase vertical motion of the rigid mass with the first beam mode may add to the strength of the second harmonic response in this excitation frequency range, particularly near $\omega/2\pi \approx 155$ Hz ($155 = 310/2$). Likewise, system resonances at 520, 625 and 830 Hz may contribute to the strength of higher harmonic responses at $\omega/2\pi \approx 173$ Hz ($173 = 520/3$), $\omega/2\pi \approx 156$ Hz ($156 = 625/4$) and $\omega/2\pi \approx 166$ Hz ($166 = 830/5$).

Other complications of the multi-dimensional system are evident in Figures 14 and 15. First, the local non-linear stiffness element affects more than just one system resonance. It is not associated with one particular mode of vibration but, rather, it affects several modes. Second, note the strong softening resonance present in the experimental results at the higher excitation level near $\omega/2\pi \approx 250$–260 Hz but not present in the theoretical simulation. Recall that the theoretical model of Section 3 considers only vertical translational motion of the system. At the lower excitation level, as shown in Figure 14, this simplified model seems to be reasonably sufficient for this excitation frequency range. However, it is clearly inadequate for the same range at the higher excitation level shown in Figure 15. This additional resonance, which was associated with some instability and

chaotic motion evident in the jagged measured response curve, is primarily due to rocking motion of the rigid body on the non-linear mount. Vertical excitation couples into rotational and horizontal translational motion due to the motion of the simply supported beam. Thus, the local non-linearity seems to have had a multi-dimensional influence as well.

5. CONCLUSIONS

The influence of a static load on the periodic response of a system with a continuous local stiffness non-linearity has been investigated theoretically and experimentally. A single-degree-of-freedom theoretical study has shown how a static load renders a hardening or softening, continuous symmetric stiffness non-linearity asymmetric. This asymmetric stiffness produces a dynamically "softening" system response under certain conditions. This intuitively agrees with some prior studies of quadratic and quadratic plus cubic non-symmetric non-linearities reported in the literature [14]. An experimental study has extended the theoretical study to multi-degree-of-freedom, multi-dimensional systems and has addressed perceived shortcomings in the literature. The experiment consisted of a linear support structure made of a simply supported beam and small mass that acts as the foot of a non-linear continuous stiffness element. On this element a rigid mass was mounted and driven by a force from an electrodynamic shaker. The system represents many practical applications in which a local stiffness non-linearity is part of an extensive system that may otherwise be modelled using linear system theory.

Various static and dynamic tests were performed on the test system and its individual components. Response to swept harmonic excitation included amplitude-dependence and sweep direction-dependence. The "softening" effect of the gravitational load on the hardening stiffness was observed experimentally. Strong superharmonic responses to sinusoidal excitation resulted from simultaneous excitation of numerous system resonances. The influence of the local non-linearity was not limited to one mode of vibration or system resonance. In summary, such a non-linearity had a rather "spatially extensive" and "frequency-extensive" effect on system behavior.

Extensions to this research that are currently in progress include consideration of other types of local non-linearities, including statically loaded discontinuous stiffness and damping elements. An attempt is also being made to improve methods for the identification of local translational and rotational non-linear parameters. The experimental procedures and results presented in this paper, along with computational tools presented in a companion paper [24], are expected to facilitate future research efforts aimed at understanding vibration and noise problems in practical mechanical systems with local non-linearities.

ACKNOWLEDGMENTS

The authors wish to acknowledge the Office of Naval Research Graduate Fellowship Program, the Center for Automotive Research at the Ohio State University, the U.S. Army Research Office (URI Grant DAAL-03-92-G-0120 ASSERT Project; Project Monitor Dr T. L. Doligalski) and the Ohio State University Graduate School for their financial support. The authors thank Hewlett-Packard and PCB Inc. for donating some of the equipment used in the study. Dr C. Padmanabhan and Dr T. E. Rook are also acknowledged for helpful advice and insight into non-linear systems and computational methods.

REFERENCES

1. Y. B. Kim, S. T. Noah and Y. S. Choi 1991 *Journal of Sound and Vibration* **144**, 381–395. Periodic response of multi-disk rotors with bearing clearances.
2. A. Kahraman and R. Singh 1991 *Journal of Sound and Vibration* **144**, 469–506. Non-linear dynamics of a geared rotor–bearing system with multiple clearances.
3. A. C. Bindemann and A. A. Ferri 1995 *Journal of Sound and Vibration* **184**, 19–34. Large amplitude vibration of a beam restrained by a non-linear sleeve joint.
4. F. Farahanchi and S. W. Shaw 1994 *Journal of Sound and Vibration* **177**, 307–324. Chaotic and periodic dynamics of a slider–crank mechanism with slider clearance.
5. C. Padmanabhan and R. Singh 1992 *Journal of Sound and Vibration* **155**, 209–230. Spectral coupling issues in a two-degree-of-freedom system with clearance nonlinearities.
6. C. Padmanabhan and R. Singh 1996 *Journal of the Acoustical Society of America* **99,** 324–334. Analysis of periodically forced non-linear Hill's oscillator with application to a geared system.
7. M. D. Bryant 1985 *Journal of Sound and Vibration* **99**, 403–414. Non-linear forced oscillation of a beam coupled to an actuator via Hertzian contact.
8. D. P. Hess and N. J. Wagh 1994 *Transactions of the American Society of Mechanical Engineers*, *Journal of Vibration and Acoustics* **116**, 474–479. Chaotic normal vibrations and friction at mechanical joints with nonlinear elastic properties.
9. G. Kim and R. Singh 1995 *Transactions of the American Society of Mechanical Engineers*, *Journal of Dynamic Systems*, *Measurement*, *and Control* **179**, 427–453. A study of passive and adaptive hydraulic engine mount systems with emphasis on non-linear characteristics.
10. H. Kojima and H. Saito 1983 *Journal of Sound and Vibration* **88**, 559–568. Forced vibrations of a beam with a non-linear dynamic vibration absorber.
11. S. Natsiavas 1992 *Journal of Sound and Vibration* **137**, 347–352. Steady state oscillations and stability of non-linear dynamic vibration absorbers.
12. B. Ravindra and A. K. Mallik 1993 *Journal of Sound and Vibration* **170**, 325–337. Performance of non-linear vibration isolators under harmonic excitation.
13. B. Ravindra and A. K. Mallik 1995 *Journal of Sound and Vibration* **182**, 345–353. Chaotic response of a harmonically excited mass on an isolator with non-linear stiffness and damping characteristics.
14. A. H. Nayfeh and D. T. Mook 1979 *Nonlinear Oscillations*. New York: John Wiley.
15. R. J. Comparin and R. Singh 1989 *Journal of Sound and Vibration* **134**, 259–290. Non-linear frequency response characteristics of an impact pair.
16. G. W. Blankenship and A. Kahraman 1995 *Journal of Sound and Vibration* **185**, 743–765. Steady state forced response of a mechanical oscillator with combined parametric excitation and clearance type non-linearity.
17. C. L. Zaretzky and M. R. M. Crespo da Silva 1994 *Journal of Sound and Vibration* **174**, 145–167. Experimental investigation of non-linear modal coupling in the response of cantilever beams.
18. L. D. Zavodney and A. H. Nayfeh 1989 *International Journal of Non-Linear Mechanics* **24**, 105–125. The non-linear response of a slender beam carrying a lumped mass to a principal parametric excitation: theory and experiment.
19. R. J. Hanson, J. M. Anderson and H. K. Macomber 1994 *Journal of the Acoustical Society of America* **96**, 1549–1556. Measurements of nonlinear effects in a driven vibration wire.
20. T. P. Valkering 1994 *Journal of Sound and Vibration* **175**, 397–422. Non-trivial dynamics in a driven string with impact non-linearity.
21. M. Urabe and A. Reiter 1966 *Journal of Mathematical Analysis and Applications* **14**, 107–140. Numerical computation of non-linear forced oscillations by Galerkin's procedure.
22. J. P. Den Hartog 1985 *Mechanical Vibrations*. Mineola, NY: Dover; reprint of fourth edition.
23. J. Pan, C. H. Hansen and J. Pan 1993 *Journal of the Acoustical Society of America* **94**, 1425–1434. Active isolation of a vibration source from a thin beam using a single active mount.
24. T. J. Royston and R. Singh 1996 *Journal of Sound and Vibration* **194**, 243–263. Periodic response of mechanical systems with local non-linearities using an enhanced Galerkin Technique.
25. N. Olsen 1994 Hewlett-Packard, Inc. Private correspondence.

APPENDIX A: LIST OF SYMBOLS

A	cross-sectional area of beam
C	mount linear damping coefficient
E	Young's modulus of beam
F_a	dynamic excitation force vector (fundamental harmonic amplitude)
F_m	static excitation force
F_y	force at flexible body/junction interface
g	gravitational constant
I	moment of inertia of beam
i	$=\sqrt{-1}$
J	junction
k	mount linearized stiffness coefficient
l_s	beam axial length
M	rigid body mass matrix
m_y	mass of small rigid body at flexible body/junction interface
N_1	number of degrees of freedom for rigid body
N_2	$=N_w$, number of degrees of freedom for flexible body
s_b	axial position of non-linear element connection point to beam
T_y	transfer function flexible body/junction interface
t	time
U	dynamic excitation force (experiment)
u	beam vertical displacement
x	rigid body displacement vector
y	displacement vector at flexible body/junction interface
ΔF_y	vertical mount operating range in the presence of dynamic excitation and gravity
δ	Dirac delta function
ρ	material density of beam
ζ_j	modal damping ratio of beam
ω'	response frequency (rad/s)
ω	excitation frequency (rad/s)